Thermoelectric Properties of 2,7-Dipyridylfluorene Derivatives in Single-Molecule Junctions

Gilles Yzambart,[†] Laura Rincón-García,[‡,§] Alaa A. Al-Jobory,[∥,⊥] Ali K. Ismael,[∥,#] Gabino Rubio-Bollinger,[‡,¶] Colin J. Lambert,*[,∥] Nicolás Agraït,*[,‡,§,¶] and Martin R. Bryce*[,†]

[†]Department of Chemistry, Durham University, Durham DH1 3LE, U.K.

[‡]Departamento de Física de la Materia Condensada and [¶]Condensed Matter Physics Center (IFIMAC) and Instituto Universitario de Ciencia de Materiales "Nicolás Cabrera" (INC), Universidad Autónoma de Madrid, E-28049 Madrid, Spain

[§]Instituto Madrileño de Estudios Avanzados en Nanociencia IMDEA-Nanociencia, E-28049 Madrid, Spain

[∥]Department of Physics, Lancaster University, Lancaster LA1 4YB, U.K.

[⊥]Department of Physics, College of Education for Pure Science, University of Anbar, Ramadi P.O. Box 55, Anbar, Iraq

[#]Department of Physics, College of Education for Pure Science, Tikrit University, Saladin P.O. Box 42, Tikrit, Iraq

Ⓢ *Supporting Information*

ABSTRACT: A series of 2,7-dipyridylfluorene derivatives have been synthesized with different substituents (2H, 2Me, 2OMe, 2CF$_3$, and O) at the C(9) position. Experimental measurements on gold|single-molecule|gold junctions, using a modified scanning tunneling microscope-break-junction technique, show that the C(9) substituent has little effect on the conductance, although there is a more significant influence on the thermopower, with the Seebeck coefficient varying by a factor of 1.65 within the series. The combined experimental and computational study, using density functional theory calculations, provides insights into the interplay of conductance and thermopower in single-molecule junctions and is a guide for new strategies for thermopower modulation in single-molecule junctions.
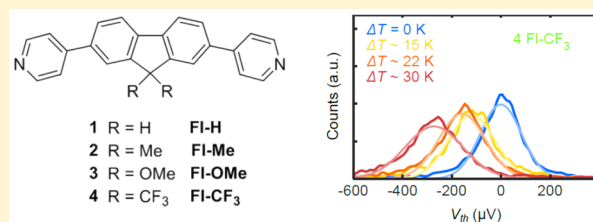
INTRODUCTION

The measurement, control, and understanding of charge transport through single molecules are of fundamental interest and are central to the development of molecular electronic devices.[1−3] A new direction for this field of research has emerged with the recent advances in techniques to measure the thermoelectric properties of organic molecules connected in electrode|single-molecule|electrode junctions.[4] This topic is providing new chemical and physical insights into charge transport at the single-molecule level. Devices with a high thermoelectric efficiency could have future applications in thermal management and the conversion of waste heat into electricity in energy harvesting applications, or for on-chip cooling in electronic devices. Molecular junctions may also be cheaper to produce and be more environmentally friendly than the present inorganic semiconducting thermoelectric devices.[5−7]

Combined experimental and theoretical studies have demonstrated that the thermopower, or Seebeck coefficient *S*, of a single-molecule junction is dependent upon chemical composition and position of the molecular energy levels with respect to the Fermi level of the metal electrodes.[8] Examples of organic molecules used in these studies include fullerenes,[9−12] benzenedithiol,[9,11,13] oligothiophenes with thiolate end-groups,[14] and molecules with amine or pyridyl anchors, namely, 1,4-diaminobenzene and π-extended analogues, and

4,4′-bipyridine.[15] Thermopower studies have addressed such factors as: substituent effects on a phenyl core and variation of the anchor group,[16] dependence on molecular length,[14,15,17] the comparison of conjugated versus nonconjugated bridging units,[14] dependence on energy alignment in the junction,[18] and quantum interference effects in the molecular backbone.[19]

The present work investigates a series of five fluorene (Fl)-based molecules **1**−**5** whose structures are shown in Figure 1. The motivation is to study the influence on transport properties in gold|single-molecule|gold junctions of different side-groups on the same backbone. All of the molecules have terminal pyridyl anchoring units at both ends, and they differ
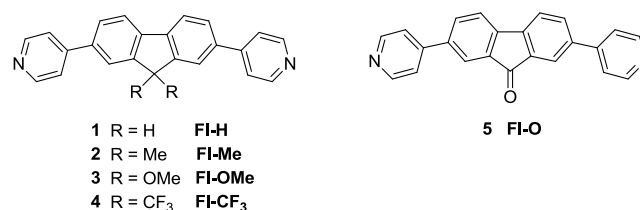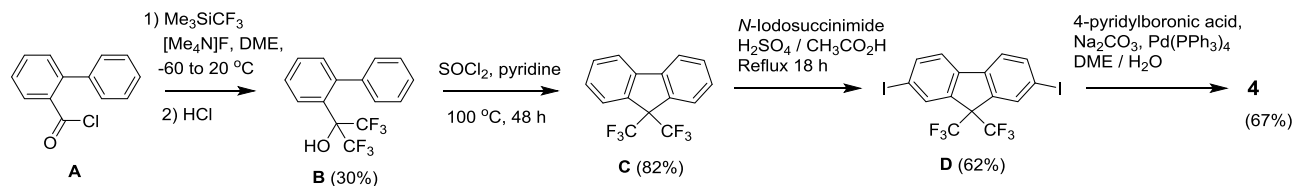

Figure 1. Structures of the molecules studied in this work.

Scheme 1. Synthetic Route to Molecule 4

only in the substituents at C(9), namely, 2H, 2Me, 2OMe, 2CF$_3$, and O (molecules **1**−**5**, respectively). Fluorene is a planarized biphenyl system, and it was chosen as the backbone for three reasons: (i) it is an established unit in single-molecule conductance studies using break-junction techniques,[20−24] although it has not been studied previously in thermopower measurements; (ii) the substituents at C(9) can be systematically varied by chemical substitution to attach electron-donating (Me or OMe) or electron-withdrawing (CF$_3$) groups; and (iii) the C(9) carbon is sp^3 hybridized in compounds **1**−**4**, so the substituents in these molecules are not directly conjugated to the π-system of the backbone. The effects of nonconjugated pendant substituents on thermopower have not, to our knowledge, been studied previously. Fluorenone compound **5** is electronically different from **1**−**4** as the pendant oxygen atom of **5** is conjugated to the backbone through the sp^2-hybridized carbon. A modified scanning tunneling microscope-break-junction (STM-BJ) technique, combined with density functional theory (DFT) calculations, has provided an in-depth analysis of the transport mechanisms in compounds **1**−**5**. The results show that the different substituents affect the thermopower but have a negligible influence on the conductance of the molecular junctions.

■ EXPERIMENTAL SECTION

Molecular Synthesis. Compounds **1**[25] and **5**[26] were synthesized as reported previously. The new fluorene derivatives **2**−**4** were synthesized in 55−67% yields from the corresponding dihalo precursors by twofold Suzuki−Miyaura reactions with 4-pyridylboronic acid. Full details of the synthesis and spectroscopic characterization are given in the Supporting Information. 2,7-Dibromo-9,9-dimethylfluorene was obtained commercially from Sigma-Aldrich. 2,7-Dibro-mo-9,9-dimethoxyfluorene was obtained in 98% yield by reaction of 2,7-dibromofluorenone with trimethylorthoformate in a refluxing mixture of concentrated sulfuric acid and methanol. The synthesis of the bis(trifluoromethyl) derivative **4** was more challenging and is shown in Scheme 1. The intermediate **C** was synthesized by a new route which is practically considerably more convenient (although lower yielding) than the literature procedure in which the CF$_3$ groups were derived from gaseous hexafluoracetone.[27] Our route from **A** to **B** uses the protocol for the synthesis of 1,1,1,3,3,3-hexafluoro-2-organyl-propan-2-ol, in which the CF$_3$ groups are introduced using trifluorotrimethylsilane (Ruppert's reagent).[28] Dehydration of **B** yielded **C** which was then iodinated to **D** as reported.[27] Finally, the palladium-catalyzed reaction of **D** with 4-pyridylboronic acid gave the target product **4**.

Sample Preparation. The compounds **1**−**5** were each deposited by drop-casting onto a 250 nm thick annealed Au(111) film on glass substrates (Arrandee, Germany). Before deposition, the Au surface was annealed at a temperature above 900 K for less than 1 min in order to have a clean polycrystalline surface (see Figure S24 in the Supporting Information). After cooling down to room temperature, the Au substrates were immersed in a 1 mM solution of **1**−**5** in dichloromethane for 30 min and then dried with streaming nitrogen. The coverage of the substrate is well below that of the monolayer, and areas can be found without molecules where junction formation is not observed.

Scanning Tunneling Microscopy. Scanning tunneling microscopy (STM) measurements were performed using a home-built STM modified to measure simultaneously the conductance G and thermopower S of single-molecule junctions.[10] Mechanically cut Au tips (0.25 mm diameter, 99.99% purity, Goodfellow) were used to contact the molecules, and STM-BJ measurements were performed in ambient conditions and at room temperature, with a bias voltage V_{bias} applied to the substrate. Single-molecule junctions were formed after breaking the Au−Au contact formed by indenting the substrate with the STM tip. The experimental technique is described in more detail in the Supporting Information.

A 1 kΩ resistor mounted in the tip support was used as a heater to establish a temperature difference ΔT between the substrate (at room temperature, T_c) and the tip (heated at a temperature $T_h > T_c$). Thermoelectric properties of each molecule were measured by applying four different ΔT's, namely, $\Delta T = T_h - T_c = 0$, ~15, ~22, and ~30 K, monitored with thermocouples in the resistor and substrate. For each ΔT, the system was allowed to stabilize for approximately 20 min before measurements were taken.

The thermopower S of single-molecule junctions was measured during the breaking of the junction, stopping the tip motion every 40−60 pm, as described in Figure S25 in the Supporting Information. The bias voltage was maintained at a fixed value $\Delta V = V_{bias} = 200$ mV during the tip motion, and it was swept twice every few picometers between $\pm \Delta V_0 = \pm 10$ mV, whereas the tip was stationary. Current−voltage (I−V) curves show a voltage offset when measuring in the presence of a temperature difference ΔT between the two Au electrodes. This voltage offset is related to the thermovoltage V_{th} of the junction (see the Supporting Information). Knowing also the temperature difference ΔT, the thermopower or Seebeck coefficient S of the junction was calculated using following eq 1

$$S = -\frac{V_{th}}{\Delta T} \tag{1}$$

Experiments were performed at zero ΔT and at three different ΔT values for each molecule to ensure a good linear fit of all of the V_{th} values, and eq 1 was used to calculate the thermopower S. The conductance is measured both from the current values while moving the tip ($V_{bias} = 200$ mV) and from the slope of the I−V curves.

Computational Details. Electronic structure calculations were performed using the DFT code SIESTA.[29] The optimum geometries of the isolated molecules were obtained by relaxing
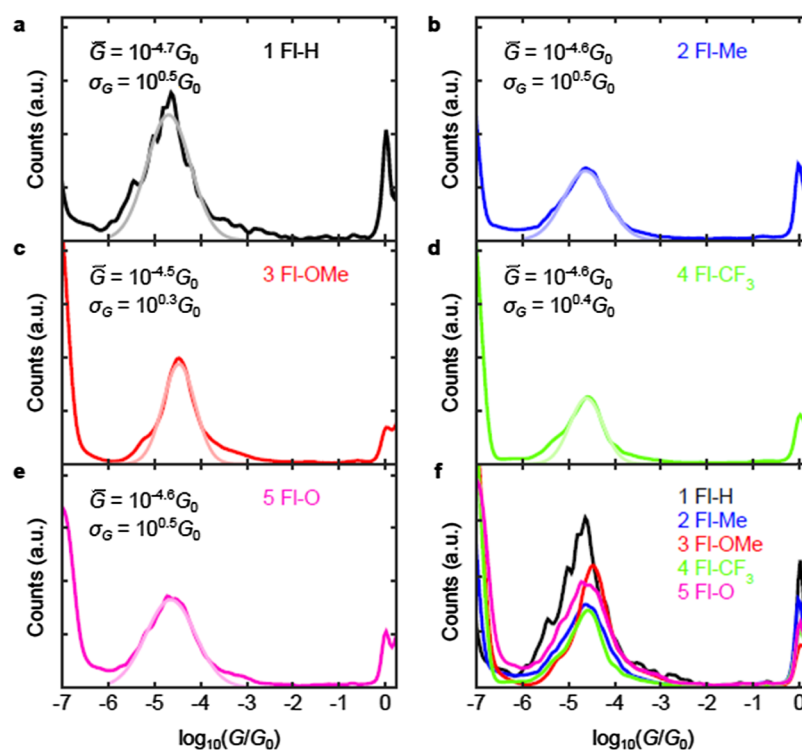
Figure 2. Conductance G 1D histograms. (a−e) Conductance G 1D histogram of each molecule and Gaussian fit of the peak corresponding to the junction values, plotted in a lighter color superimposed to the histograms. $\bar{G}$ and σ_G in each panel are the expected value (most probable value) of the conductance and the standard deviation of the fit, respectively. (f) Conductance G 1D histograms of all of the molecules. Each histogram is normalized with its total number of measured values.

the molecules until all forces on the atoms were less than 0.05 eV/Å. The SIESTA calculations employed a double-zeta plus polarization orbital basis set and norm-conserving pseudopotentials; an energy cutoff of 250 rydberg defined the real space grid, and the exchange correlation functional was LDA. To calculate their electrical conductance, the molecules were attached to gold leads via the pyridyl anchor groups. The leads were constructed of 6 layers of Au(111) each containing 30 gold atoms, and the optimum binding distance was calculated to be 2.4 Å (Figure S3 in the Supporting Information) between the terminal nitrogen atoms and a "top" gold atom. A Hamiltonian describing this structure was produced using SIESTA, and the zero-bias transmission coefficient $T(E)$ was calculated using the Gollum code.[30] Further details are provided in the Supporting Information.

It is well known that DFT frequently underestimates the highest occupied molecular orbital (HOMO)−lowest unoccupied molecular orbital (LUMO) gap,[31,32] and from Table S1 in the Supporting Information, it is clear that the calculated gaps are less than the optically measured gaps. To overcome this deficiency, a scissor correction is performed by diagonalizing the molecular submatrix of the full Hamiltonian, then shifting the eigenvalues below and above the Fermi energy such that the new HOMO−LUMO gap matches the experimental value of the isolated molecule. Finally, the diagonalized matrix is transformed back to the original basis to obtain the corrected full Hamiltonian.

■ RESULTS AND DISCUSSION

In order to find the most probable value of the conductance of each molecule $\bar{G}$, one-dimensional (1D) histograms were plotted with all of the conductance values obtained from each junction break (Figure 2). A peak can be identified in the histograms corresponding to the Au−Au contact (at $G = G_0$, where G_0 is the quantum of conductance, $G_0 = 2e^2/h$). The values on the left of the histograms correspond to the noise level of the system, below $10^{-6.5}$ G_0. An extra peak, not present when measuring only Au−Au contacts, is observed that corresponds to the molecular junction formation. While the tip is retracting from the surface, a molecule may connect both electrodes. As the tip separates further from the surface, the conductance remains almost constant resulting in a conductance plateau in the conductance G versus displacement Δz curves, instead of decreasing exponentially, as occurs with Au−Au tunneling. Figure S26 in the Supporting Information shows the two-dimensional histograms for each molecule built from the G versus Δz curves. These plateaus create a junction-characteristic peak in the G 1D histograms. Using a Gaussian fit, $\bar{G}$ (the expected value) and σ_G, the standard deviation, are obtained.

A very similar conductance value was obtained for each of the molecules **1−5**, as a consequence of the similar transport pathways in each molecule, which are located predominantly on the conjugated backbone. The data are shown in Figure 2 and summarized in Table 1. The values we report are similar to those previously reported for other fluorene derivatives with thiol anchor groups, using different break-junction techniques.[21,22]

To study the thermoelectric properties of the Au|molecule| Au junctions, the thermovoltage V_{th} was measured as the junction breaks using four temperature differences between tip and sample, namely, $\Delta T = 0, \sim 15, \sim 22,$ and ~ 30 K. Figure 3a shows the equivalent thermal circuit taking into account the contribution from the lead connecting the heated tip (see

Table 1. Measured Conductances (Column 2), Conductance Histogram Widths (Column 3), and Seebeck Coefficients (Column 4)

molecule	$\log_{10}(\overline{G}/G_0)$	standard deviation $\log_{10}(\sigma_G/G_0)$	$\overline{S}$ (μV/K)
1 Fl–H	−4.7	0.5	−5.5
2 Fl–Me	−4.6	0.5	−8.6
3 Fl–OMe	−4.5	0.3	−7.4
4 Fl–CF$_3$	−4.6	0.4	−8.0
5 Fl–O	−4.6	0.5	−9.0

further details in the Supporting Information). More than one set of measurements was carried out for each ΔT and each molecule. Figure 3 shows a plot of V_{th} 1D histograms with the values of all of the sets of measurements at each ΔT and the fit to a Gaussian distribution (plotted in a lighter color superimposed on the histograms in Figure 3).

Figure 4 shows the mean value $\overline{V}_{th}$ of each set of measurements as a function of the temperature difference ΔT (empty circles). The error bars of $\overline{V}_{th}$ are the standard deviations $\sigma_{V_{th}}$ obtained from the Gaussian fit of each set of measurements. The linear fit shown in Figure 4 is obtained by fitting all of the individual V_{th} values independently, without taking into account if one set of measurements has more or less points than another. The slope of this fit corresponds to the thermopower S of the molecule, and the values are shown as an inset in each plot. The relative error of S obtained with this fit is smaller than 2% in all cases, meaning that there are sufficient measurements to give a reliable value of S.

The Seebeck coefficients of the different molecules are summarized in Table 1, with a variation from −5.5 μV/K in the lowest case (compound **1**) to −9.0 μV/K, in the highest case (compound **5**). The experimental results show that the variation of the C(9) substituents has little effect on the conductance, while having a more significant effect on the thermopower, increasing the Seebeck coefficient by a factor of 1.65. The data show that all of the substituents at C(9) slightly increase the thermopower (compared to the unsubstituted molecule **1**) and the values for **2−5** do not follow a trend in the electron-donating or electron-withdrawing effect of the substituent. The sign of S for all of the compounds **1−5** is negative, consistent with the Fermi level being closer to the LUMO than to the HOMO.[4]

Figure 5 shows the DFT-predicted transmission coefficients for the molecules, as a function of $E − E_M$, where E_M is the energy of the middle of the HOMO−LUMO gap. Note that the slope of $T(E)$ near the mid-gap is not zero because $T(E)$ is rather asymmetric within the gap. This asymmetry arises because the HOMOs of these molecules are degenerate, as shown in Figures S4−S8 in the Supporting Information. Indeed, as described by the Breit−Wigner formula[33] when on-resonance the transmission coefficient of a symmetric molecule should be unity, unless the resonant level is degenerate. This is why the HOMO transmission resonances in Figure 5 are much less than unity, whereas the nondegenerate LUMO resonances are close to unity. There is no frontier orbital distribution on the pendant group at C(9) for molecules **1−4** (Figures S4−S7), whereas for molecule **5**, there is a contribution of the HOMO, LUMO, and LUMO + 1 on the fluorenone oxygen atom (Figure S8). Nevertheless, in common with those of **1−4**, the orbitals of **5** are predominantly located on the backbone, and as shown in Figure 5, the transmission function of **5** is almost identical with those of **1−4** within the HOMO−LUMO gap. This explains the similar experimental results for
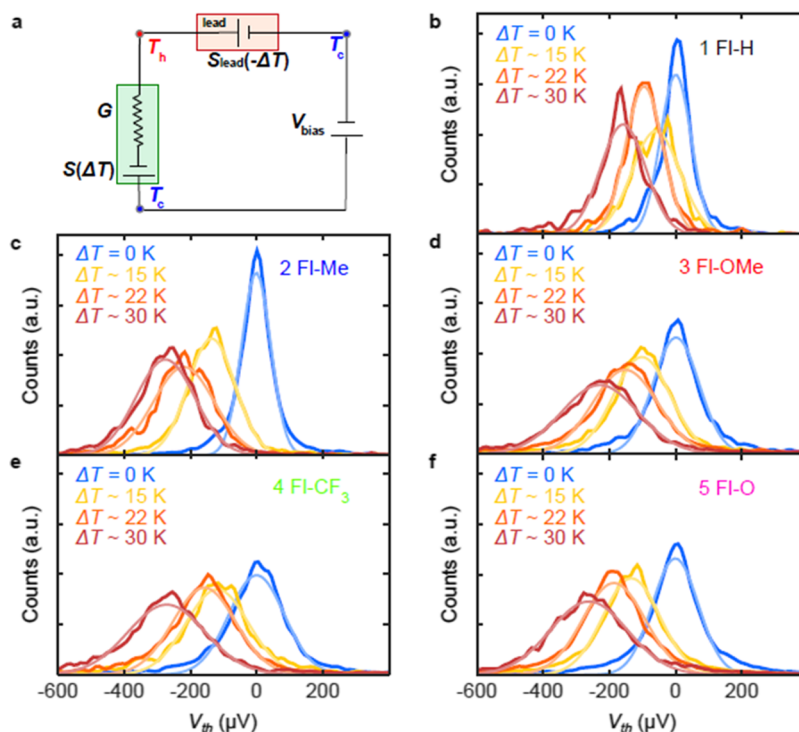

Figure 3. Thermal circuit and thermovoltage V_{th} 1D histograms for compounds **1−5**. (a) Equivalent thermal circuit. Besides the thermovoltage produced in the molecular junction, there is another contribution from the lead that connects the heated tip, equal to $S_{lead}(-\Delta T)$, where S_{lead} is the thermopower of the lead (see further details in the Supporting Information). (b−f) Thermovoltage V_{th} 1D histograms of each molecule and Gaussian fits plotted in a lighter color superimposed on the histograms.
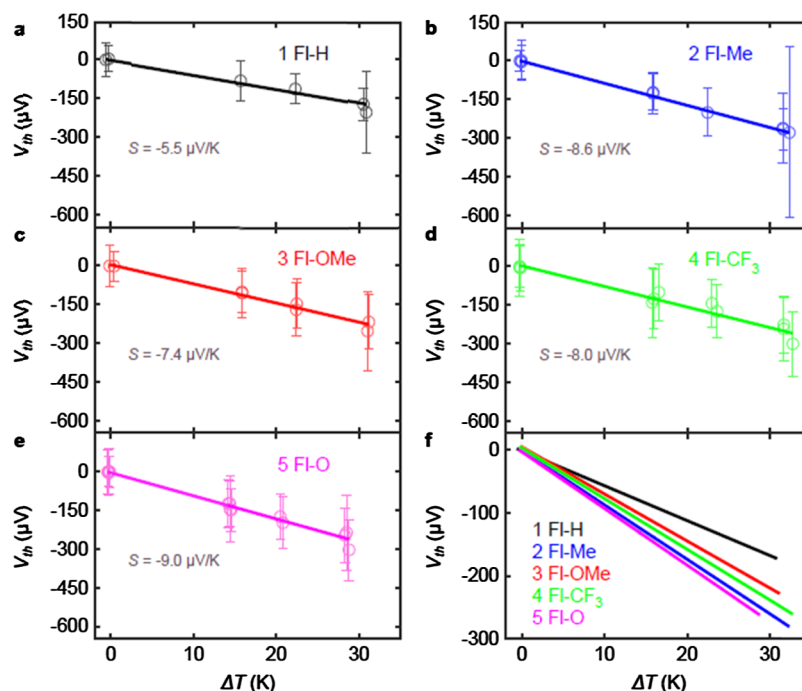
Figure 4. Thermopower S values. (a–e) Linear fit to all of the V_{th} values for molecules **1–5**, respectively, to obtain the thermopower S of each molecule, which is the slope of this fit (values are shown in each plot). The empty circles correspond to the mean thermovoltage value $\overline{V_{th}}$ obtained from the Gaussian fit of each set of measurements. The error bars of $\overline{V_{th}}$ are the standard deviations $\sigma_{V_{th}}$ and are typically between 73 μV for $\Delta T = 0$ K to 135 μV for $\Delta T \approx 30$ K (as can be seen in the figure). (f) Linear fit of all of the V_{th} values shown in panels a–e, combined for comparison.
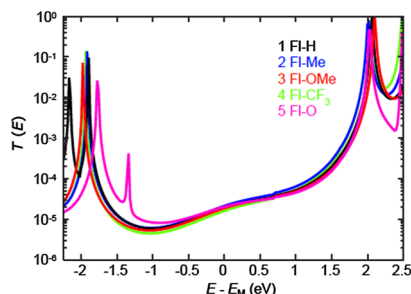

Figure 5. Transmission coefficients $T(E)$ for molecules **1–5** after scissor corrections.

the conductance of **1–5**. The transmission function $T(E)$ includes the effect of contacts unlike the electrical conductance (which is obtained by thermally averaging $T(E)$) does not depend on temperature. Therefore, a low-temperature measurement is unlikely to reveal further differences between the molecules.

Figure 6 shows a comparison between the theoretical conductances and Seebeck coefficients obtained from the transmission curves. In agreement with the experiment, the Seebeck coefficient is negative because of the presence of the pyridyl anchors, which tend to move the LUMO toward the Fermi energy. Because the Fermi energy is determined in part by environmental factors, theoretical results are shown for two values of the Fermi energy, namely, $E_F = E_M$ and $E_F = E_M - 0.3$ eV. This window captures the experimental values of both conductance and thermopower. The differences between experiment and theory most likely arise from the fact that the Fermi energy (relative to frontier orbital energies) varies from molecule to molecule. Table 2 shows that almost exact
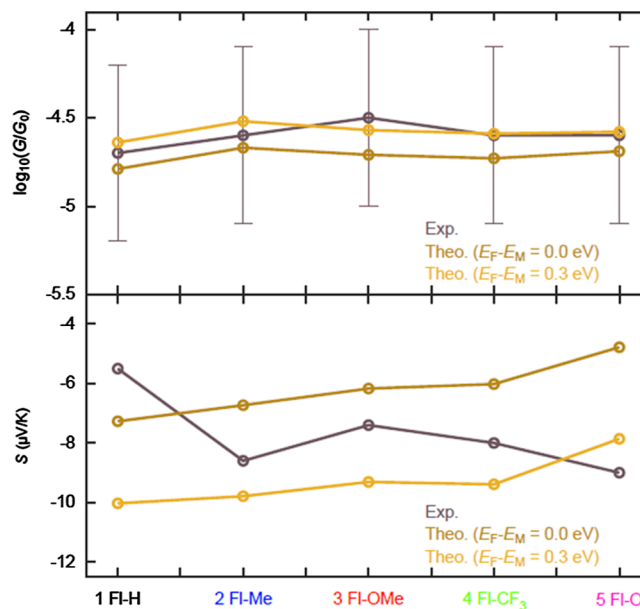

Figure 6. Conductance and Seebeck theoretical and experimental results. Top panel: Comparison between measurements and calculations of conductance. The error bars correspond to the standard deviation shown in Table 1. Bottom panel: Comparison between measurements and calculations of Seebeck coefficients.

agreement between theory and experiment can be obtained if small variations in E_F occur between the molecules.

■ CONCLUSIONS

A series of fluorene derivatives **1–5** have been synthesized, and their conductance and thermopower have been measured in gold|single-molecule|gold junctions using a modified STM-BJ

Table 2. Theoretical Results Obtained Using the Fermi Energies Shown in Column 2

molecule	$E_F - E_M$ (eV)	Exp. $\overline{S}$ (μV/K)	Theo. $\overline{S}$ (μV/K)	Exp. $\log_{10}(G/G_0)$	Theo. $\log_{10}(G/G_0)$
1 Fl—H	0.40	−5.5	−6.8	−4.7	−4.6
2 Fl—Me	0.10	−8.6	−8.6	−4.6	−4.6
3 Fl—OMe	0.16	−7.4	−7.4	−4.5	−4.6
4 Fl—CF$_3$	0.10	−8.0	−8.1	−4.6	−4.6
5 Fl—O	−0.15	−9.0	−9.1	−4.6	−4.7

technique. By systematically varying the pendant group, the Seebeck coefficient can be varied from −5.5 μV/K for molecule **1** to −9 μV/K for molecule **5** which is an increase of almost 80%, whereas the electrical conductance remains essentially unchanged across the series of molecules. This combined experimental and computational study demonstrates that fluorene is a suitable backbone unit for measurements of thermopower and that nonconjugated pendant substituents can influence the thermopower of a molecular system—a topic that has not been studied previously. Future strategies could be to attach substituents at different positions on the fluorene ring for thermopower enhancement in single-molecule junctions and for studying quantum interference effects through a fluorene backbone.

ASSOCIATED CONTENT

ⓢ Supporting Information
The Supporting Information is available free of charge on the ACS Publications website at DOI: 10.1021/acs.jpcc.8b08488.

> Synthesis and characterization details of the new molecules; methods and results for the single-molecule conductance and thermopower measurements for compounds **1**−**5**; and computational methods and data (PDF)

AUTHOR INFORMATION

Corresponding Authors
*E-mail: c.lambert@lancaster.ac.uk (C.J.L.).
*E-mail: nicolas.agrait@uam.es (N.A.).
*E-mail: m.r.bryce@durham.ac.uk (M.R.B.).

ORCID ⓘ
Gabino Rubio-Bollinger: 0000-0001-7864-8980
Colin J. Lambert: 0000-0003-2332-9610
Martin R. Bryce: 0000-0003-2097-7823

Author Contributions
G.Y., L.R.-G., A.A.A.-J., and A.K.I. contributed equally to this work. The manuscript was written with contributions of all authors. All authors have given approval to the final version of the manuscript.

Notes
The authors declare no competing financial interest.

REFERENCES
(1) Cuevas, J. C.; Scheer, E. *Molecular Electronics: An Introduction to Theory and Experiment*; World Scientific Publishing Co. Pte. Ltd.: Singapore, 2010.
(2) Xiang, D.; Wang, X.; Jia, C.; Lee, T.; Guo, X. Molecular-Scale Electronics: From Concept to Function. *Chem. Rev.* **2016**, *116*, 4318−4440.
(3) Leary, E.; La Rosa, A.; González, M. T.; Rubio-Bollinger, G.; Agraït, N.; Martín, N. Incorporating Single Molecules into Electrical Circuits. The Role of the Chemical Anchoring Group. *Chem. Soc. Rev.* **2015**, *44*, 920−942.
(4) Rincón-García, L.; Evangeli, C.; Rubio-Bollinger, G.; Agraït, N. Thermopower Measurements in Molecular Junctions. *Chem. Soc. Rev.* **2016**, *45*, 4285−4306.
(5) Malen, J. A.; Yee, S. K.; Majumdar, A.; Segalman, R. A. Fundamentals of energy transport, energy conversion, and thermal properties in organic-inorganic heterojunctions. *Chem. Phys. Lett.* **2010**, *491*, 109−122.
(6) Zhang, Q.; Sun, Y.; Xu, W.; Zhu, D. Organic Thermoelectric Materials: Emerging Green Energy Materials Converting Heat to Electricity Directly and Efficiently. *Adv. Mater.* **2014**, *26*, 6829−6851.
(7) Dubi, Y.; Di Ventra, M. Colloquium: Heat Flow and Thermoelectricity in Atomic and Molecular Junctions. *Rev. Mod. Phys.* **2011**, *83*, 131−155.
(8) Baheti, K.; Malen, J. A.; Doak, P.; Reddy, P.; Jang, S.-Y.; Tilley, T. D.; Majumdar, A.; Segalman, R. A. Probing the Chemistry of Molecular Heterojunctions Using Thermoelectricity. *Nano Lett.* **2008**, *8*, 715−719.
(9) Yee, S. K.; Malen, J. A.; Majumdar, A.; Segalman, R. A. Thermoelectricity in Fullerene-Metal Heterojunctions. *Nano Lett.* **2011**, *11*, 4089−4094.
(10) Evangeli, C.; Gillemot, K.; Leary, E.; González, M. T.; Rubio-Bollinger, G.; Lambert, C. J.; Agraït, N. Engineering the Thermopower of C60 Molecular Junctions. *Nano Lett.* **2013**, *13*, 2141−2145.
(11) Lee, S. K.; Ohto, T.; Yamada, R.; Tada, H. Thermopower of Benzenedithiol and C60 Molecular Junctions with Ni and Au Electrodes. *Nano Lett.* **2014**, *14*, 5276−5280.
(12) Rincón-García, L.; Ismael, A. K.; Evangeli, C.; Grace, I.; Rubio-Bollinger, G.; Porfyrakis, K.; Agraït, N.; Lambert, C. J. Molecular Design and Control of Fullerene-Based Bi-Thermoelectric Materials. *Nat. Mater.* **2016**, *15*, 289−293.
(13) Reddy, P.; Jang, S.-Y.; Segalman, R. A.; Majumdar, A. Thermoelectricity in Molecular Junctions. *Science* **2007**, *315*, 1568−1571.
(14) Chang, W. B.; Mai, C.-K.; Kotiuga, M.; Neaton, J. B.; Bazan, G. C.; Segalman, R. A. Controlling the Thermoelectric Properties of Thiophene-Derived Single-Molecule Junctions. *Chem. Mater.* **2014**, *26*, 7229−7235.
(15) Kim, T.; Darancet, P.; Widawsky, J. R.; Kotiuga, M.; Quek, S. Y.; Neaton, J. B.; Venkataraman, L. Determination of Energy Level Alignment and Coupling Strength in 4,4′-Bipyridine Single-Molecule Junctions. *Nano Lett.* **2014**, *14*, 794−798.
(16) Baheti, K.; Malen, J. A.; Doak, P.; Reddy, P.; Jang, S.-Y.; Tilley, T. D.; Majumdar, A.; Segalman, R. A. Probing the Chemistry of Molecular Heterojunctions Using Thermoelectricity. *Nano Lett.* **2008**, *8*, 715−719.
(17) Malen, J. A.; Doak, P.; Baheti, K.; Tilley, T. D.; Segalman, R. A.; Majumdar, A. Identifying the Length Dependence of Orbital

Alignment and Contact Coupling in Molecular Heterojunctions. *Nano Lett.* **2009**, *9*, 1164−1169.

(18) Guo, S.; Zhou, G.; Tao, N. Single Molecule Conductance, Thermopower, and Transition Voltage. *Nano Lett.* **2013**, *13*, 4326−4332.

(19) Miao, R.; Xu, H.; Skripnik, M.; Cui, L.; Wang, K.; Pedersen, K. G. L.; Leijnse, M.; Pauly, F.; Wärnmark, K.; Meyhofer, E.; et al. Influence of Quantum Interference on the Thermoelectric Properties of Molecular Junctions. *Nano Lett.* **2018**, *18*, 5666−5672.

(20) Hines, T.; Diez-Perez, I.; Hihath, J.; Liu, H.; Wang, Z.-S.; Zhao, J.; Zhou, G.; Müllen, K.; Tao, N. Transition from Tunneling to Hopping in Single Molecular Junctions by Measuring Length and Temperature Dependence. *J. Am. Chem. Soc.* **2010**, *132*, 11658−11664.

(21) Haiss, W.; Wang, C.; Jitchati, R.; Grace, I.; Martín, S.; Batsanov, A. S.; Higgins, S. J.; Bryce, M. R.; Lambert, C. J.; Jensen, P. S.; et al. Variable Contact Gap Single-Molecule Conductance Determination for a Series of Conjugated Molecular Bridges. *J. Phys.: Condens. Matter* **2008**, *20*, 374119.

(22) Vonlanthen, D.; Mishchenko, A.; Elbing, M.; Neuburger, M.; Wandlowski, T.; Mayor, M. Chemically Controlled Conductivity: Torsion-Angle Dependence in a Single-Molecule Biphenyldithiol Junction. *Angew. Chem., Int. Ed.* **2009**, *48*, 8886−8890.

(23) Klausen, R. S.; Widawsky, J. R.; Su, T. A.; Li, H.; Chen, Q.; Steigerwald, M. L.; Venkataraman, L.; Nuckolls, C. Evaluating Atomic Components in Fluorene Wires. *Chem. Sci.* **2014**, *5*, 1561−1564.

(24) Gantenbein, M.; Wang, L.; Al-Jobory, A. A.; Ismael, A. K.; Lambert, C. J.; Hong, W.; Bryce, M. R. Quantum Interference and Heteroaromaticity of *Para-* and *Meta-*Linked Bridged Biphenyl Units in Single Molecular Conductance Measurements. *Sci. Rep.* **2017**, *7*, 1794.

(25) Zhao, X.; Li, X.; Zhao, Y.; Zhang, J.; Pan, J.; Zhou, J. Amplified Spontaneous Emission from 2,7-Bis(4-pyridyl)fluorene-Doped DNA-Cetyltrimethyl Ammonium Complex Films. *Opt. Eng.* **2013**, *52*, 106109.

(26) Niu, Z.; Li, D.; Liu, D.; Xia, D.; Zou, Y.; Sun, W.; Li, G. Syntheses, Electrochemical Behaviors, Spectral Properties and DFT Calculations of Two 1,3-Dithiole Derivatives. *Chem. Res. Chin. Univ.* **2014**, *30*, 425−430.

(27) Amara, J. P.; Swager, T. M. Conjugated Polymers with Geminal Trifluoromethyl Substituents Derived from Hexafluoroacetone. *Macromolecules* **2006**, *39*, 5753−5759.

(28) Babadzhanova, L. A.; Kirij, N. V.; Yagupolskii, Y. L.; Tyrra, W.; Naumann, D. Convenient Syntheses of 1,1,1,3,3,3-Hexafluoro-2-organyl-propan-2-ols and the Corresponding Trimethylsilyl Ethers. *Tetrahedron* **2005**, *61*, 1813−1819.

(29) Soler, J. M.; Artacho, E.; Gale, J. D.; García, A.; Junquera, J.; Ordejón, P.; Sánchez-Portal, D. The SIESTA method for*ab initio*order-N*materials simulation. *J. Phys.: Condens. Matter* **2002**, *14*, 2745−2779.

(30) Ferrer, J.; Lambert, C. J.; García-Suárez, V. M.; Manrique, D. Z.; Visontai, D.; Oroszlany, L.; Rodríguez-Ferradás, R.; Grace, I.; Bailey, S. W. D.; Gillemot, K.; et al. GOLLUM: a Next-Generation Simulation Tool for Electron, Thermal and Spin Transport. *New J. Phys.* **2014**, *16*, 093029.

(31) Lof, R. W.; van Veenendaal, M. A.; Koopmans, B.; Jonkman, H. T.; Sawatzky, G. A. Band gap, excitons, and Coulomb interaction in solid*C60. *Phys. Rev. Lett.* **1992**, *68*, 3924−3927.

(32) Hung, Y.-C.; Jiang, J.-C.; Chao, C.-Y.; Su, W.-F.; Lin, S.-T. Theoretical Study on the Correlation between Band Gap, Bandwidth, and Oscillator Strength in Fluorene-Based Donor−Acceptor Conjugated Copolymers. *J. Phys. Chem. B* **2009**, *113*, 8268−8277.

(33) Claughton, N. R.; Leadbeater, M.; Lambert, C. J. Theory of Andreev Resonances in Quantum Dots. *J. Phys.: Condens. Matter* **1995**, *7*, 8757−8784.